Australasian Physical & Engineering Sciences in Medicine (2019) 42:585–598
https://doi.org/10.1007/s13246-019-00760-7

SCIENTIFIC PAPER

Assessment of the accuracy of truebeam intrafraction motion review (IMR) system for prostate treatment guidance

Guneet Kaur[1] · **Joerg Lehmann**[1,2,3] · **Peter Greer**[1,2] · **John Simpson**[1,2]

Received: 7 October 2018 / Accepted: 30 April 2019 / Published online: 13 May 2019
© Australasian College of Physical Scientists and Engineers in Medicine 2019

Abstract

Intrafraction motion review (IMR), a real-time 2D, motion management feature of the Varian Truebeam™ incorporates triggered imaging, automatic fiducial marker detection and automatic beam hold. With the increasing adoption of high dose per fraction stereotactic body radiotherapy (SBRT) this system provides a potential means to ensure treatment accuracy. The goal of this study was therefore to investigate and quantify key performance characteristics of IMR for prostate treatment guidance. Phantom experiments were performed with a custom Computerized Imaging Reference Systems, Inc (CIRS) pelvis phantom with implanted gold seeds and the Hexamotion™ 5D motion platform. The system accuracy was assessed statically and under typical prostate motion trajectories. The IMR functionality and marker detectability was tested under different anatomical conditions and with different imaging acquisition modes. Imaging dose for triggered imaging modes was determined using an ionisation chamber based on IPEMB dose calibration protocol for kV energies. For zero displacement, the IMR demonstrated submillimeter agreement with the known position. Similarly, dynamic motion differences between the IMR reported position and 2D trajectory displacement were within 1 mm. Static displacement in the anterior direction was reported by IMR as sinusoidal motion on the x-axis (kV angle). The 2D nature of IMR limits the ability to detect motion out of the plane of the kV image detector. Using typical clinical imaging settings, imaging dose determined at the patient surface was 2.58 mGy/frame and the corresponding IMR displayed dose was 2.63 mGy/frame. The methodology used was able to quantify the accuracy of the IMR system. The IMR was able to accurately and consistently report fiducial positions within the limitations inherent of a 2D system. IMR is fully integrated with the Truebeam system with an easy to use and efficient workflow and is clinically beneficial especially within the context of SBRT.

Keywords Intrafraction motion monitoring · Prostate cancer · Dose measurement

Introduction

Prostate cancer is one of the most common malignancies in the western male population. External beam radiation therapy (EBRT) is an important treatment option for prostate cancer however intrafraction motion of the prostate during EBRT delivery has been a concern and limitation for treatment of prostate cancer. It has been shown that intrafraction motion can cause under-dosing of the target and overdosing organs at risk [1]. This motion is accounted for by using an expansion margin around the clinical target volume (CTV) [2]. The size of the margin is important; if the margin is too small it could result in compromised target coverage; if the margin is too large it could result in overdosing of adjacent organs at risk. In prostate EBRT, implanted fiducial markers are often used for daily image-guided setup. In order to monitor and manage intrafraction motion, real time assessment

✉ John Simpson
John.Simpson@calvarymater.org.au

Guneet Kaur
Guneet.Kaur@calvarymater.org.au

Joerg Lehmann
Joerg.Lehmann@calvarymater.org.au

Peter Greer
peter.greer@newcastle.edu.au

[1] Department of Radiation Oncology, Calvary Mater Newcastle Hospital, Newcastle, NSW, Australia

[2] School of Mathematical and Physical Sciences, Faculty of Science and IT, University of Newcastle, Newcastle, NSW, Australia

[3] Institute of Medical Physics, University of Sydney, Sydney, NSW, Australia

of prostate position is required and one such method is to use the fiducial markers as a prostate surrogate and to track them over the course of treatment. Ideally, one would also wish to interrupt the treatment when motion exceeds a certain tolerance [3]. Characterisation of prostate intrafraction motion has shown that intrafraction motion could be could be irregular and unpredictable [4].

A number of modalities have previously been used for understanding and tracking intrafraction motion such as portal imaging with and without implanted fiducials, in-room computed tomography (CT) (cone-beam CT), 4D ultrasound [5, 6], megavoltage (MV) imaging, cine-magnetic resonance imaging [7] and 4D localization using implanted electromagnetic beacons [8]. These systems are effective for intrafraction motion monitoring to varying degrees; however, they do not allow for continuous monitoring or they require a separate system, which comes with additional cost, operator training and may not integrate well with the clinical patient treatment workflow. Thus, the use of already available integrated linac based imaging systems is highly desirable. One study has explored tracking of fiducial markers via kilovoltage and megavoltage imaging and a dynamic multileaf collimator (MLC) beam tracking system [9]. This system is easy to implement as the method utilizes the kV/MV imaging system that is already available on linac treatment machines. However, it is not (yet) commercially available. Another method utilising kV/MV systems addressed the limitation where the fiducial markers are obstructed by the MLC leaves by retracting the leaves at imaging points. The method has been shown to be feasible for intrafraction motion monitoring during VMAT treatments where there is less MLC leaf modulation however it does require modification of the treatment plan [10]. Kilovoltage Intrafraction monitoring system is a novel Intrafraction real-time tumour localization modality. It provides 3D positional information of fiducial markers [11].

The Truebeam linear accelerator (Varian Medical Systems, Palo Alto, CA, USA) can be optionally equipped with integrated imaging and motion management technology, which allows for monitoring and visual verification of fiducial motion known as intrafraction motion review (IMR). IMR incorporates triggered kilovoltage (kV) imaging; automatic fiducial marker detection and auto beam hold (ABH) functionality. Triggered kV imaging is the ability to acquire planar kV images at certain intervals during treatment delivery. Differing triggering modes available with the IMR system are based on either elapsed time, gantry angle increments or delivered monitor units (MU).

IMR works by segmenting fiducial markers in the acquired kV images and comparing them to on-the-fly digitally reconstructed radiograph (DRR) marker positions that have been pre-defined from the planning CT. A user defined tolerance diameter (or a custom contour) is applied for fiducial position acceptance. This allows IMR to track motion of the markers to determine if the markers are in or out of tolerance. If selected, IMR can also automatically interrupt treatment if the magnitude of motion exceeds the set tolerance.

Although IMR has been available clinically for several years, investigations of its performance have not been reported in the literature. With the adoption of prostate stereotactic body radiotherapy with highdoses per fraction the clinical use of IMR is likely to increase. The goal of this study was therefore to investigate and quantify key physical performance characteristics of IMR. These include the ability of the system to segment markers under varying anatomical conditions, the positional accuracy of IMR, the impact of the geometric limitations of the system, the effect of auto-beam hold on dose delivery and the imaging dose to the patient as a function of imaging technique. A companion paper to this one will report the optimisation and clinical significance of the user defined tolerance diameter. It will also include a comparison to 3D capable position monitoring methods.

Methods and materials

Measurement equipment

The accuracy of IMR for marker segmentation was investigated using a custom anthropomorphic pelvic prostate phantom (Computerized Imaging Reference Systems (CIRS) Inc., Norfolk, VA, USA) implanted with three gold seeds (cylindrical fiducials markers of 1.0 mm diameter and 3.0 mm length) and placed on a custom made platform connected to a programmable Hexamotion 5D motion platform (ScandiDos, Uppsala, Sweden).

This was utilized to generate both simple test movements and complex patient-measured three dimensional prostate motion trajectories. A CT scan of the phantom was acquired for VMAT planning and reference images using an Aquilion large bore CT scanner (Canon Medical System, Japan) with 140 kV and 1.25 mm slice thickness. All measurements were performed on a Varian Truebeam™ 2.5 STx linear accelerator equipped with an on-board kilovoltage imaging system using an amorphous silicon (aSi) flat-panel imager and an aS1200 megavoltage electronic portal imaging device (EPID) Fig. 1. The treatment delivery parameters used to perform the series of experiments were adapted from a clinical study (Prometheus) and are shown in Table 1.

Intrafraction motion review system

There are various components and stages to the IMR system.

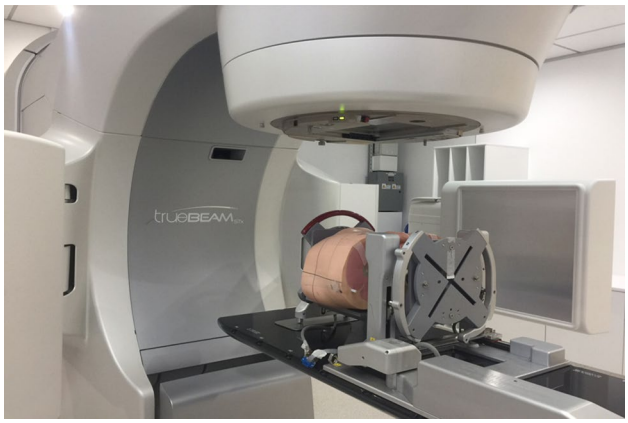

Fig. 1 Phantom Setup with a CIRS pelvis phantom and Hexamotion 5D stage on the treatment couch of Varian Truebeam

Table 1 Treatment parameters used for this study, based on clinical treatment parameter used in the department for prostate VMAT treatment

Treatment parameters	
Treatment type	Dual arc volumetric modulated arc therapy (VMAT)
Fractionation	SBRT Boost (2 × 10 Gy)
Fiducials	Three cylindrical gold fiducial markers (1 mm diameter × 3 mm length)
Energy	10X-FFF
Dose rate [MU/min]	2400 (nominal)

Triggered imaging

To apply IMR, a triggered kV imaging mode needs to be selected. Triggering can be initiated either by time, gantry angle or monitor units (MU) during treatment. The minimum trigger intervals; in time, gantry and MU mode are 3 s, 10º and 120 MU respectively. The imaging parameters such as kV, mAs are pre-selected by the user.

Fiducial marker detection

IMR identifies the location of fiducial markers in the kV triggered images using multiple "imaging cascades". Image filtering and segmentation is applied to each cascade and fiducial candidates are generated and ranked according to the expected location of the markers from the planning CT. The process of fiducial selection from the candidate set is known as the "automatic fiducial marker detection".

The user defined a tolerance region (usually circular) for acceptance in the plane of the imager but with dimensions referenced to same plane at the isocentre level. The selection of the tolerance region, defines the region of interest. If the marker has been found within the tolerance region then the identified fiducial marker position and the search area are displayed in a green colour. If the algorithm detects the fiducial marker outside the tolerance, IMR displays the identified marker position and the search area in a red colour. If the algorithm does not detect a fiducial marker then the search area is displayed in an orange colour.

Auto-beam holds (ABH)

Another feature of IMR is "Auto Beam Hold" (ABH). If selected by the user the ABH feature controls the treatment beam based on the location of fiducial markers in the kV triggered images compared to the expected positions. If any fiducial is found to be outside the user set tolerance region then the beam is paused. The beam is also paused if any fiducial markers cannot be found. The ABH puts the treatment beam on hold just prior to acquisition of each triggered image in order to eliminate the effect of MV scatter on the kV image. This causes a pause in gantry motion as well during VMAT delivery which increases treatment time. When operated in "time" triggered mode, kV images continue to be acquired and the machine will automatically resume treatment once all markers are found to be within the tolerance region. In other modes the treatment is manually restarted.

Impact of patient size and imaging parameters on marker detectability

The sensitivity and specificity of the automatic marker segmentation in relation to patient size and kV imaging parameters was investigated. This information is important in order to set imaging parameters that result in effective detection of the fiducial markers while minimising patient dose. Solid Water™ (RMI, Madison WI) blocks were added to the CIRS phantom in the lateral direction to increase the effective patient size. In addition, the IMR image acquisition parameters were varied to study the effect of imaging technique on marker detection (Table 2).

Positional accuracy of IMR

Phantom studies were performed to determine the positional accuracy of the IMR system. These were reported as the difference between IMR reported fiducial positions and the

Table 2 Imaging acquisition parameters used to assess marker detectability

Imaging acquisition parameter	
kV energies	100 and 125 kV
mAs	7.5, 15 and 30 mAs
Field size	6 × 6 cm^2 and 10 × 10 cm^2

known position of the fiducial markers. Before each measurement, the CIRS phantom was placed on the Hexamotion platform and aligned to the planned treatment isocentre using CBCT.

Firstly, a series of simple displacements were introduced to the CIRS phantom; zero displacement, 3 mm displacement in the anterior direction, 3 mm displacement in the left lateral direction, 3 mm displacement in the superior direction and 3 mm displacement in all three directions. These choices were based on previous reports showing that anteroposterior (AP) and Superior- inferior (SI) directions are the most common directions for prostate motion [12].

Next, three 3D motion trajectories were applied to the CIRS phantom based on previously measured patient prostate motion patterns. The trajectories used were obtained from real prostate motion trajectories obtained from prostate cancer patients undergoing conventional fractionated intensity modulated radiotherapy and acquired using kilovoltage intrafraction motion monitoring software [11]. The three were chosen for their different patterns of motion and are shown in Fig. 2

IMR images were acquired using the time-based triggering mode with the minimum setting of 3 s in order to achieve maximal temporal resolution, resulting in one image approximately every 17.5° of the gantry rotation. The imaging parameters were those previously used in a prostate clinical trial (Prometheus) and are listed in Table 3.

For these tests, the auto beam hold (ABH) was disabled to ensure continuous delivery. Marker displacement was reported in the two-dimensional imager coordinate system as a function of kV source angle [(−) 180°–180°]. The imager coordinate system allocates the x-axis to the cross plane (combination of patient anterior–posterior and patient left–right displacement depending on kV source angle) and the y-axis to the patient superior–inferior direction.

The procedure was repeated three times for each case and the result was obtained by averaging the three results. Results were normalised to the initial position of the

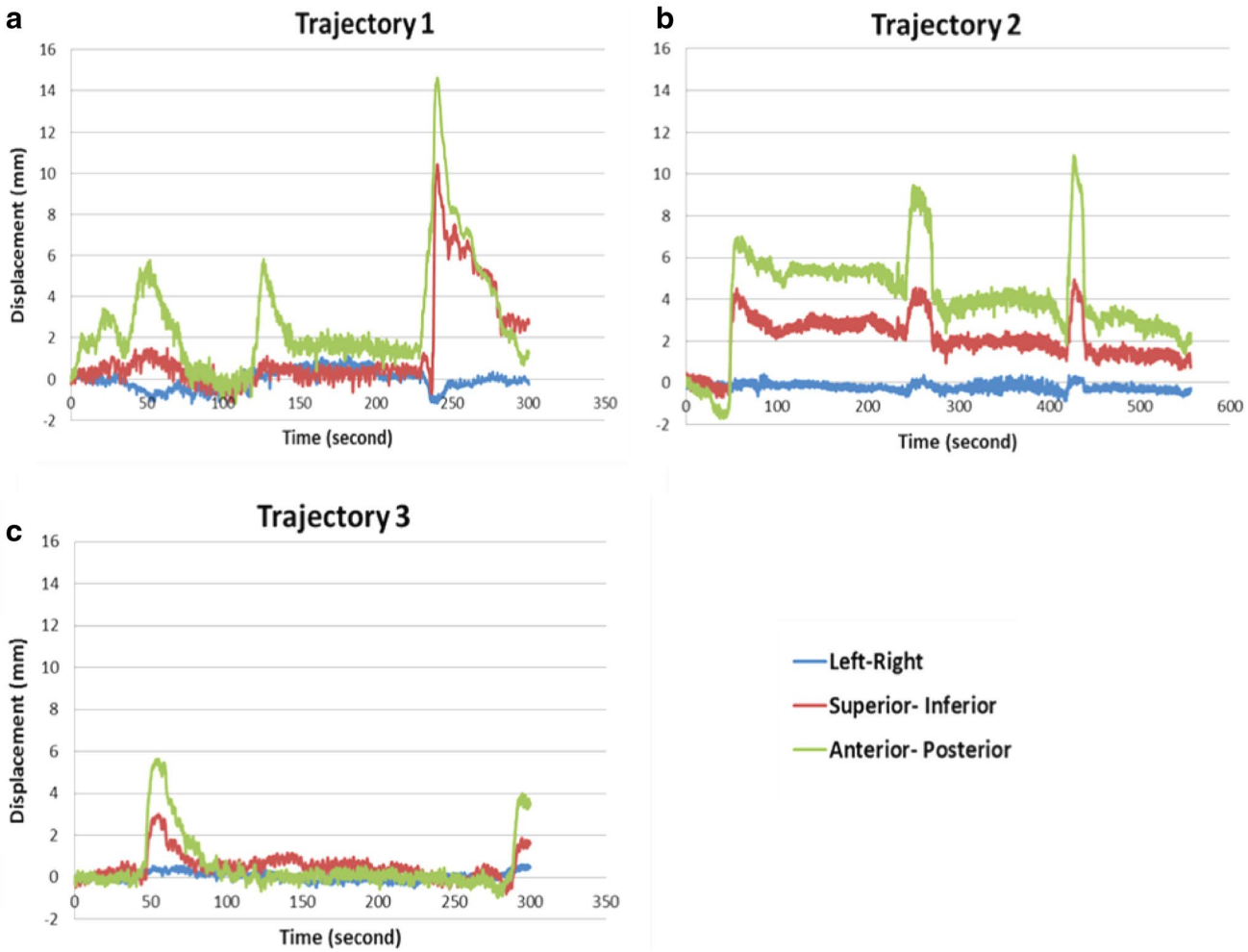

Fig. 2 Real prostate motion trajectories used to determine IMR accuracy

Table 3 Imaging acquisition parameter used for prostate VMAT treatment in the department

Imaging acquisition parameter	
kV imager position (distance from iso-center)	80 cm
Nominal energy	125 kV
milliampere-second (mAs)	15 mAs
Field size	10×10 cm^2
Anatomy	Pelvic lateral
Size	Large
Trigger	Time-3 s
Imaging type	Single
Tolerance region	Default-Diameter 5 mm

phantom to eliminate any initial systematic setup error from the CBCT positioning. In order to directly compare the IMR reported displacement with known 3D displacements, the spatial coordinates of the trajectories were projected into the 2D kV imager coordinate system by geometric transformation.

IMR allows the user to visually compare the location of the marker and indicates if the markers have moved out of the tolerance region. The IMR estimated marker positions are stored in a combined log file. The log file contains the marker position in the imager coordinate system based on pixel number. It reports the estimated marker positon and the expected marker positon based on the planned CT position for the given gantry angle. The reported positions are in image coordinates (pixels) which are converted to the physical coordinates (mm) for comparison with the known position. The IMR estimated positions were determined from the combined log files using MATLAB (R2015b, Mathworks, Massachusetts, USA).

Effect of auto beam hold on the dose delivery

To investigate the beam hold feature of ABH a 3 mm displacement was introduced in the anterior direction. The effect of ABH (MV interruption) on the treatment delivery was measured using a 0.22 cc Farmer ionization chamber placed near the centre of the phantom. The imaging and treatment settings were those used clinically and are provided in Tables 1 and 3. The prostate test plan used was based on a dual arc SBRT- VMAT plan (Arc1: 140°–220° and Arc2: 220°–140°). The dose was measured with both ABH enabled and disabled using triggering modes "gantry angle" and "time" (18° and 3 s respectively). The dose was measured for both arcs separately and the total treatment delivery time was recorded. The treatment time was also measured for the zero displacement case for comparison.

Effect of MV scatter on marker detection

To test the effect of MV scatter on marker detection, two sets of images were acquired; one with the MV beam interrupted during kV image acquisition and one with the MV continuously on. For both cases, images were acquired using a "gantry mode" of 17.5°. The imaging acquisition parameters used to acquire these images were 125 kV; 15 mAs; kV blade size 10×10 cm^2.

To compare differences in image quality due to the presence of MV scatter the contrast to noise ratio (CNR) was calculated for ten images both with and without the MV beam on during kV image acquisition as [13]:

$$\mathrm{CNR} = \frac{(\mathrm{mean}_{\mathrm{marker}} - \mathrm{mean}_{\mathrm{background}})}{\sqrt{((\sigma_{\mathrm{marker}})^2 + (\sigma_{\mathrm{background}})^2)}} \quad (1)$$

A Student's *t* test was performed to assess the statistical significance between the two cases. P value <0.05 was considered statically significant.

Evaluation of imaging dose as a function of IMR imaging parameters

Experiments were performed to determine the dose received by the patient as a function of triggered imaging parameters (kV, mAs and kV blade size). The imaging dose per frame and dose for a typical SBRT treatment used in the department were determined using a published formalism [14, 15] based on the IPEMB dose calibration protocol for kV energies [16]. A Farmer-type ion chamber without a build-up cap was used to measure beam half-value layer (HVL) using aluminium sheets, and absolute dose measurements in air.

The imaging dose was measured using the IMR trigger mode "time" with a trigger interval of 3 s. Imaging acquisition parameters were as described in Table 2.

The 10×10 cm^2 kV blade size was chosen as it represents the blade size used for imaging in many treatments performed in the department. In addition, a 6×6 cm^2 kV blade size was investigated as this represents a reduced imaging field size that would cover the prostate PTV with all fiducials within the field. Ion chamber imaging dose measurements were obtained at the cardinal gantry angles of the treatment arc (270°, 0° and 90°) and at each of these angles, ten frames were acquired. The average chamber reading per frame was calculated. Measurements were repeated three times.

The imaging dose per frame was calculated as the dose to water at the surface using Eq. (2)

$$D_{w,z=0,iso} = MN_k\left(\frac{\mu_{en}}{\rho}\right)B_w \quad (2)$$

where $D_{w,z=0,iso}$ is the dose to the water at the surface for one frame; M the ion chamber reading per frame corrected for temperature and pressure; N_k the ion chamber air kerma calibration factor; $\left(\frac{\mu_{en}}{\rho}\right)$ is the mass energy absorption coefficient and B_w is the backscatter factor. The values for $\left(\frac{\mu_{en}}{\rho}\right)$ and B_w have been interpolated using the IPEMB protocol, the kV setting and the measured HVL.

The dose per frame at PTV depth 15.3 cm $D_{w,z=15.3,iso}$ was also calculated using Eq. 3

$$D_{w,z=15.3\text{ cm, iso}} = D_{w,z=0,\text{ iso}} \times ISL \times PDD \times FSF \quad (3)$$

where ISL is the inverse square law factor, PDD is the percentage depth dose and FSF is the field size factor. The tissue depth of 15.3 cm was selected based on Crocker et al., as the reported median prostate plan isocenter depth [14].

The total imaging dose per treatment was calculated using Eq. 4

$$D_{\text{treatment}} = D_{w,z=15.3,iso} \times N \quad (4)$$

where N is the number of imaging frames.

Results

Impact of patient size and imaging parameters on marker detectability

The sensitivity of marker detection versus phantom size is shown in Fig. 3. The number of frames with at least one undetected marker is plotted as a function of phantom size for combinations of kV and mAs settings. For a given phantom size, the reliability of marker detection increases with increasing kV and mAs. For the 40 cm wide phantom, all but the lowest exposure setting (100 kV, 7.5 mAs) was able to detect all markers for 100% of the time.

Positional accuracy of IMR

Figure 4 displays the IMR reported position of one of the gold seeds (Marker 1) for static displacements as a function of kV source angle. It illustrates the 2D nature of the IMR system in which the anterior and left displacements are reported as a sinusoidal marker displacement in the x-axis with the maximum amplitude equalling the magnitude of the actual displacement (3 mm). The superior-inferior direction motion (panel y-axis) was fully described. It was also observed that the detectability of the markers in the phantom was 100%, except when marker 2 and 3 overlap in the kV image, the IMR algorithm is unable to distinguish between the two markers and therefore does not report displacements for marker three at this angle.

To determine the 2D accuracy of the IMR system, the known 3D marker positions were transformed to the imager plane of reference for each of the static displacement and dynamic motion tests. The results of both the static and dynamic tests appear in Tables 4 and 5 respectively, which shows the mean difference and the standard deviation between the IMR reported positions and the expected positions. For the zero displacement case the mean difference was 0.17 ± 0.50 mm and -0.67 ± 0.07 mm for x-axis and y-axis respectively. The difference between the IMR reported positions and the expected positions, in both the static and dynamic tests demonstrates the submillimeter agreement. In the case of 3 mm static displacement, the mean difference (± 1

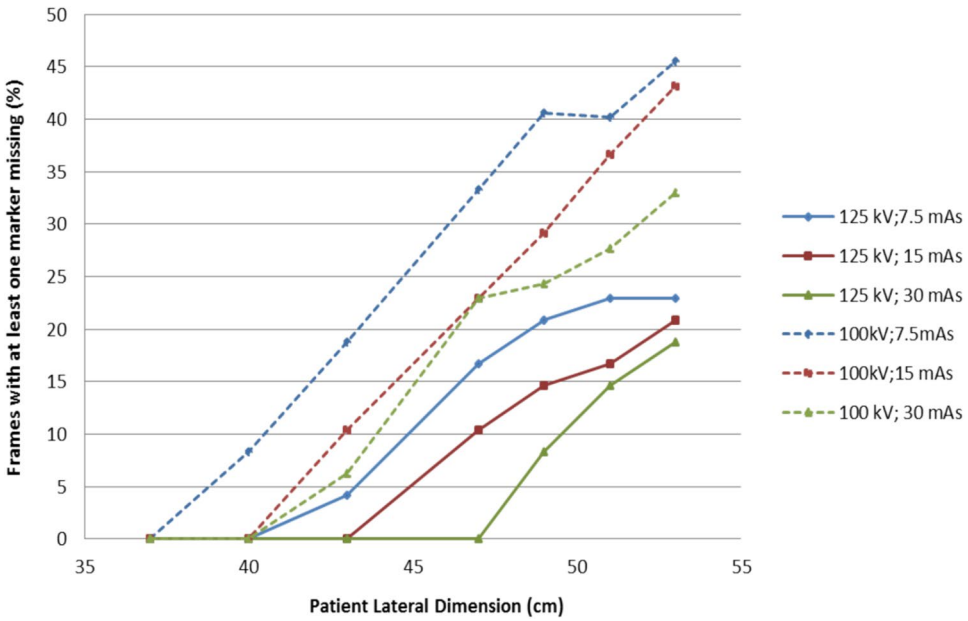

Fig. 3 Number of frames for which at least one marker has not been detected as a function of patient size and imaging acquisition parameter

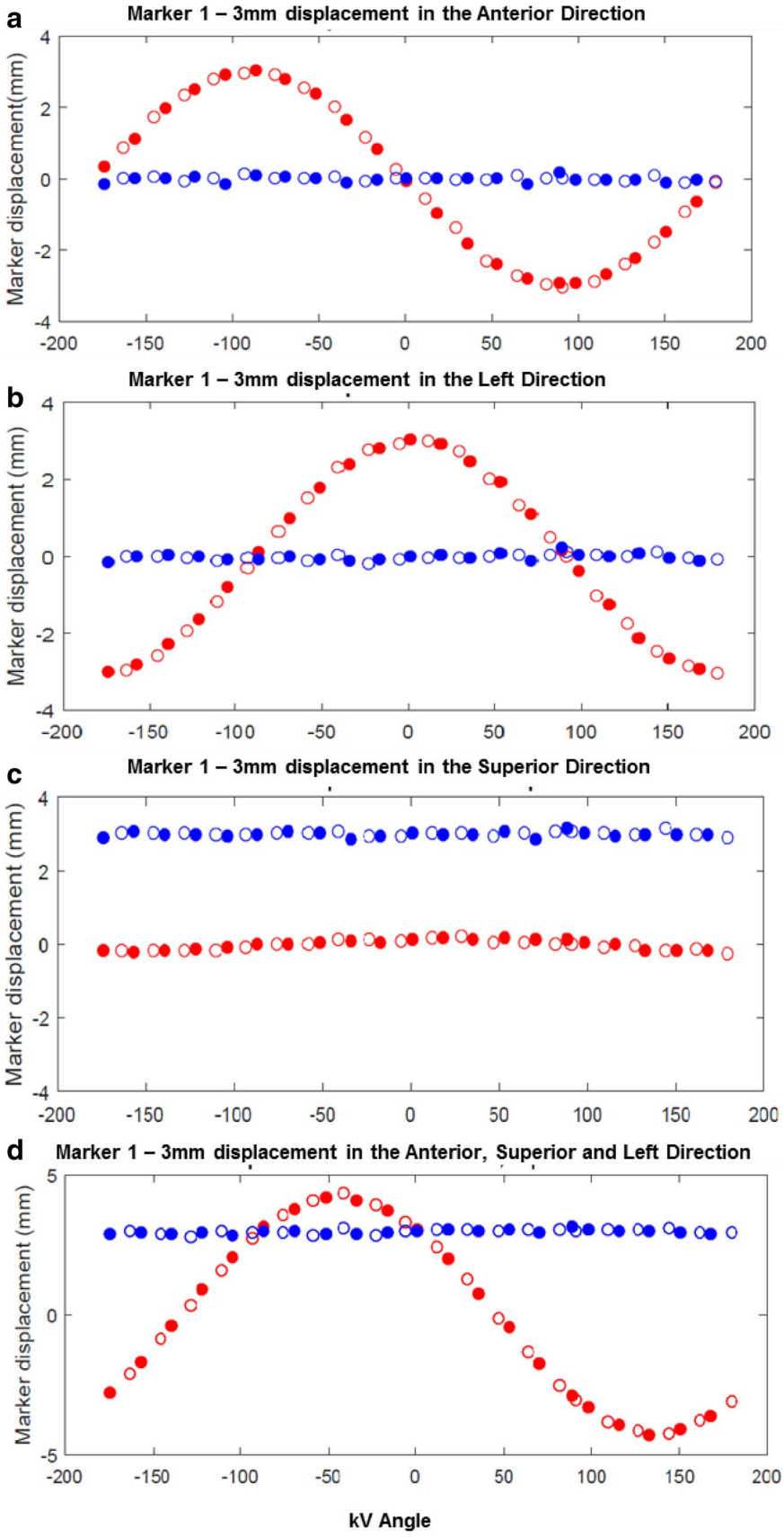

Fig. 4 IMR reported marker positions for a 3 mm static displacement in the anterior direction (top), left direction (2nd from top), superior direction (2nd from bottom) and all 3 direction (bottom). The red dots show the x-axis position and blue show the y-axis position as reported by IMR. Filled dots are from Arc 1 (counter-clockwise) and open dots from Arc 2 (clockwise) of the treatment

Table 4 Static motion test result: difference between the 2D projected static motion and IMR reported position of the the centroid positions of the markers as a mean difference and standard deviation

Static displacement	x axis Difference mean ± SD (mm)	y axis Difference mean ± SD (mm)
Zero displacement	0.17 ± 0.50	− 0.67 ± 0.07
3 mm Displacement anterior direction	− 0.004 ± 0.11	− 0.003 ± 0.04
3 mm Displacement superior direction	0.02 ± 0.13	0.008 ± 0.036
3 mm Displacement left direction	0.013 ± 0.57	0.03 ± 0.04
3 mm in Displacement in each Ant, Sup and Left direction	− 0.02 ± 0.09	0.03 ± 0.04

Table 5 Dynamic Motion test results: difference between the 2D projections of dynamic trajectory and IMR reported position as a mean difference and standard deviation

Dynamic trajectory	x axis Difference Mean ± SD (mm)	y axis Difference Mean ± SD (mm)
Trajectory 1	0.05 ± 0.35	− 0.19 ± 0.56
Trajectory 2	− 0.02 ± 0.19	− 0.02 ± 0.25
Trajectory 3	0.14 ± 0.87	− 0.13 ± 0.39

standard deviation) for motion in the anterior direction was − 0.06 ± 2.11 mm and − 0.00 ± 0.06 mm for the x-axis and y-axis respectively; superior direction was − 0.02 ± 0.13 mm and − 0.08 ± 0.30 mm; and the left direction was − 0.03 ± 2.15 mm and − 0.03 ± 0.07 mm. Combining results for all three directions the difference was − 0.08 ± 2.99 mm and − 0.03 ± 0.07 mm for the x-axis and y-axis respectively. For the dynamic test, the mean difference for trajectory 1 was 0.05 ± 0.35 mm and − 0.19 ± 0.56 mm, for trajectory 2 was − 0.02 ± 0.19 mm and − 0.02 ± 0.19 mm, for trajectory 3 was 0.14 ± 0.87 mm and − 0.13 ± 0.39 mm for the x-axis and y-axis, respectively.

The IMR reported position and the known position are plotted in Figs. 5, 6 and 7 for the 3D dynamic trajectories as a function of time. The IMR default circular tolerance region was used in the measurements with a tolerance diameter of 5 mm. It was observed that for excursions larger than 5 mm the system was unable to detect the markers (orange state) instead of indicating it as outside tolerance (red state). This indicates that the tolerance diameter functions as a search region diameter as well as a tolerance region diameter. This can be seen in Fig. 5 between approximately 240–255 s, in Fig. 6 between approximately 60–100 s and in Fig. 7 between approximately 60-100 s.

Effect of auto beam hold on the dose delivery

To ensure that the use of ABH does not adversely affect the delivered treatment dose the integrated ion chamber response near the isocentre of the phantom was measured for three different IMR modes and compared to treatment delivery without IMR kV imaging. The position of the phantom remained constant between deliveries. The treatment time increased for the modes involving MV beam off, not only due to the beam off time but also to allow the gantry to rotate back to the position just prior to where the MV beam was turned off. The absorbed dose to the water to determine the effect of auto beam hold appears in Table 6. The difference in the absorbed dose to water for different scenarios (ABH disabled, ABH with "Gantry angle" mode, ABH with "Time" mode) from the treatment without IMR was directly proportional to the number of imaging frames acquired with no changes in dose resulting from MV interruptions.

Effect of MV scatter on marker detection

Kilovoltage images were acquired with and without the MV beam active during image acquisition using the parameters listed in Table 2. For both cases, IMR was able to detect the markers. CNR was measured for ten images at different gantry angles with ABH disabled and enabled. The mean CNR was 47.0 for images acquired in the presence of the MV beam (ABH disabled) and 49.7 for images without MV beam (ABH enabled). There was no statistical significant difference in the image quality (p-value = 0.51) between the two cases (Fig. 8).

Evaluation of imaging dose as a function of IMR imaging parameters

Imaging dose as function of kV energies and mAs

The measured half-value-layer (HVL) for the two kV imaging energies and the absorbed dose per frame are recorded in Table 7 for each kV energy and mAs. The measured imaging dose at the patient surface (zero depth, 125 kV and 15 mAs) of 2.58 mGy/frame was found to be in good agreement with the corresponding IMR displayed dose of 2.63 mGy/frame.

Imaging dose as a function of field size

Using clinical prostate SBRT treatment plan image acquisition parameters, the imaging dose per frame at the isocentre for the 10×10 cm^2 and 6×6 cm^2 field size was found to be 2.58 mGy/frame and 2.29 mGy/frame, respectively.

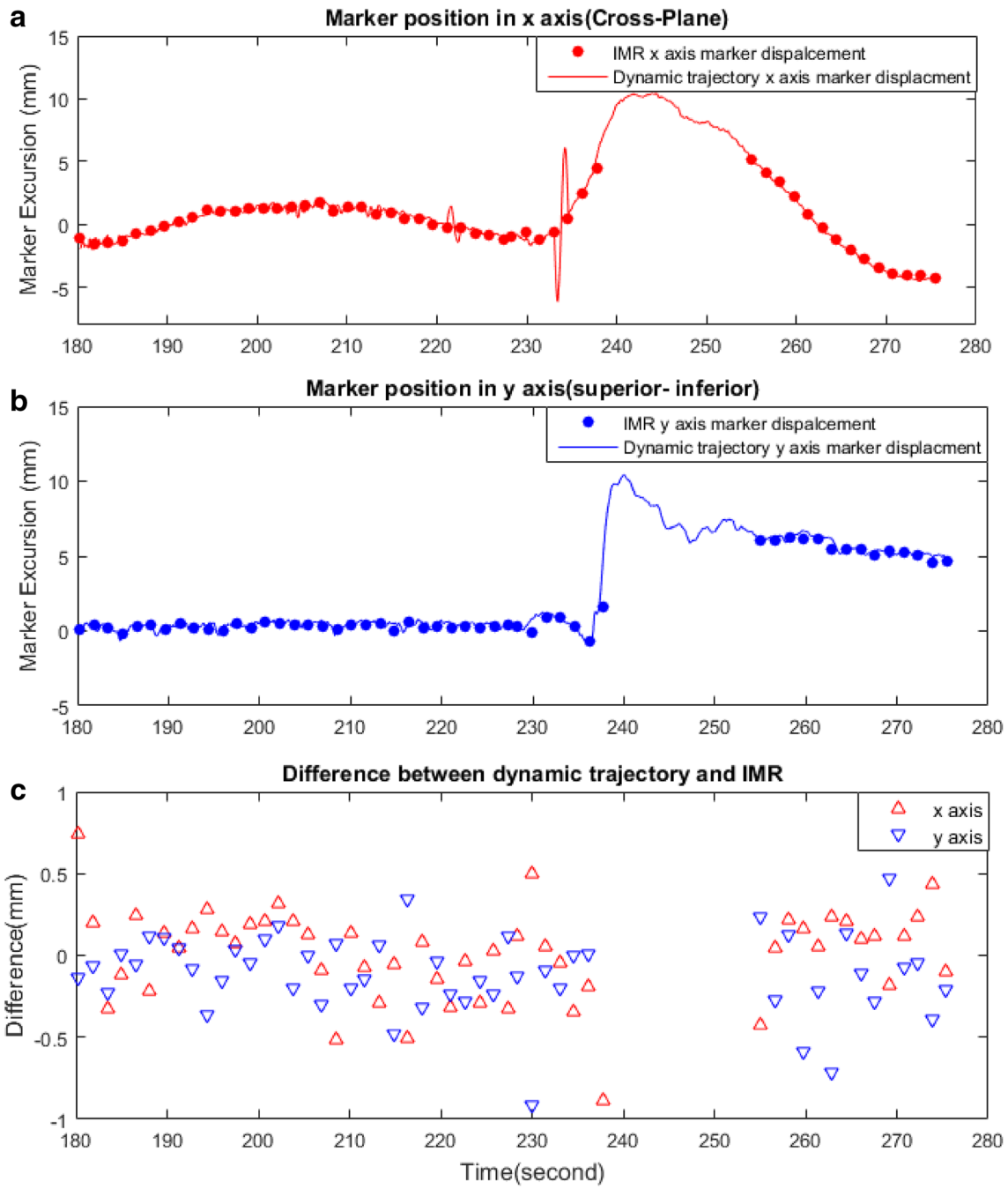

Fig. 5 Trajectory 1, actual (2D converted) and IMR reported centroid displacemnt in the x-axis (upper), y-axis (mid) and difference plot (lower)

Discussion

The results demonstrated that IMR was able to segment the fiducials under all conditions except on the rare occasion they overlapped. Even with the largest phantom dimension of 43 cm, which corresponded to the largest actual patient from our clinical dataset, the fiducials were fully detected with appropriate adjustment of the acquisition parameters.

The phantom studies found the absolute positional accuracy of the IMR system to be within 1 mm for both static and dynamic motion analysis when compared with the 2D projection of the 3D marker position information. The static motion data analysis (Fig. 4) illustrated how the inherent 2D nature of IMR limits its ability to determine motion perpendicular to the kV image detector and how this results in reduced sensitivity to detect out of tolerance displacements. As shown by the sinusoidal curves in Fig. 4,

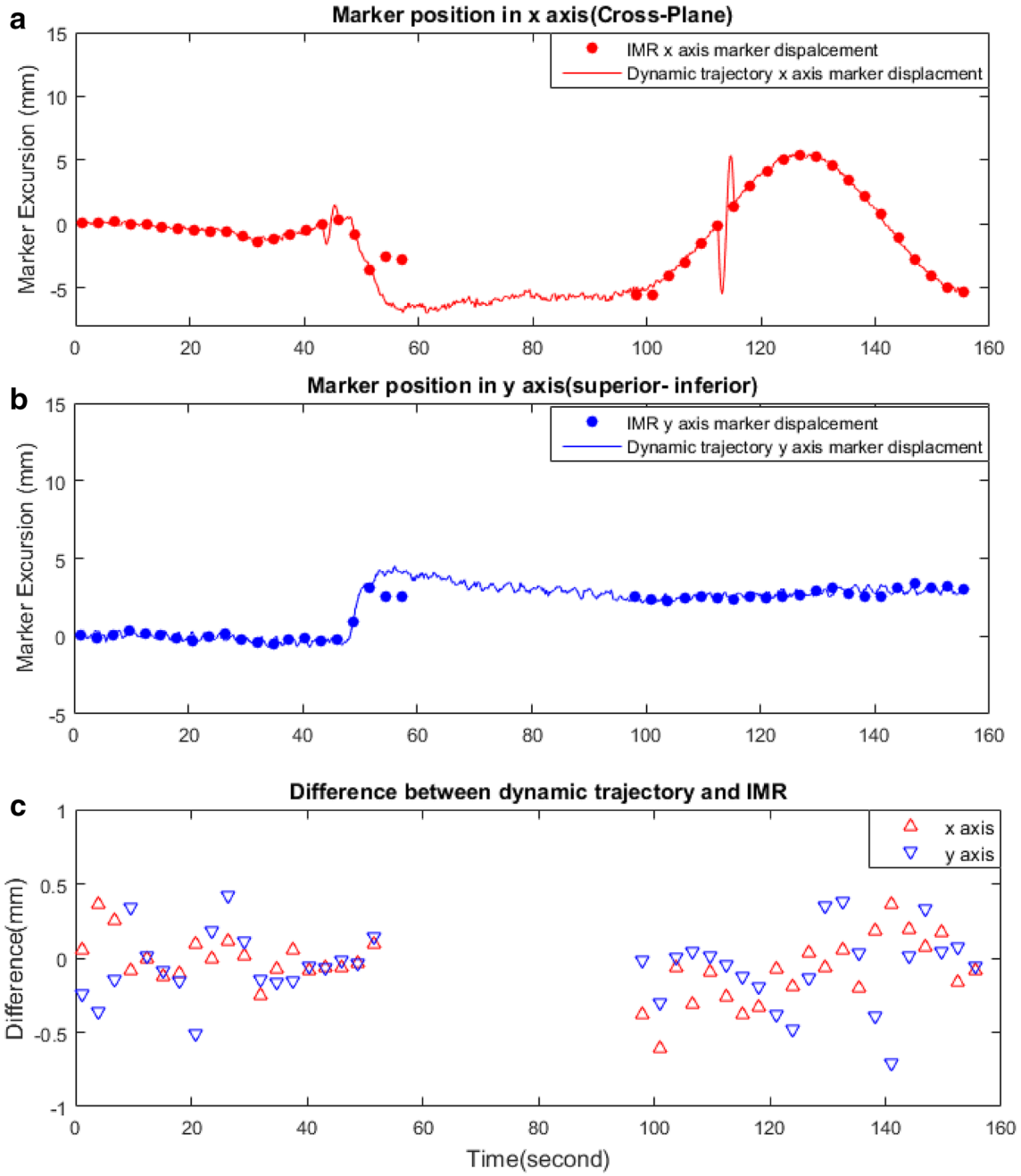

Fig. 6 Trajectory 2, actual (2D converted) and IMR reported centroid displacement in the x-axis (upper), y-axis (mid) and difference plot (lower)

the actual magnitude of the shifts in the anterior–posterior and left–right directions is only fully appreciated when the motion is in the plane, parallel to the kV detector. The loss of fiducial marker position information due to this limitation may have a clinical impact, as any motion perpendicular to the kV image detector will not be detected. For VMAT treatments, this can result in delayed detection of tumour motion during treatment. Thereby this can affect target coverage and sparing of organs at risk. The clinical impact of this effect is somewhat mitigated by the fact that all motion in the superior-inferior direction will be correctly observed by IMR, and any motion often has multiple components. Additionally, the impact can be compensated for by reducing the tolerance diameter; however the tolerance diameter must be sufficient to exclude clinically insignificant effects such as respiratory motion and noise.

As mentioned in the introductions, there are 3D capable radiographic imaging based methods available, including

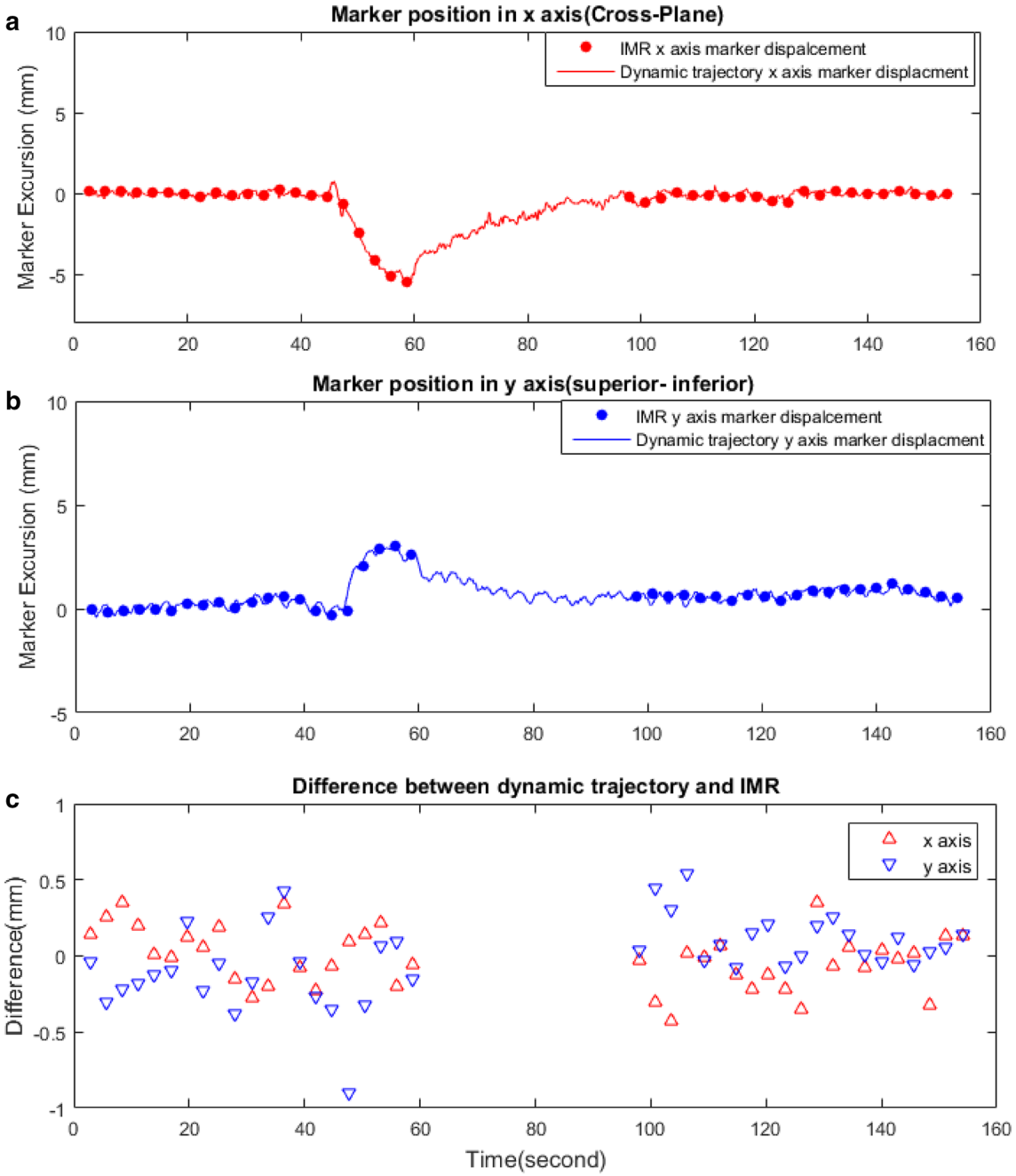

Fig. 7 Trajectory 3, actual (2D converted) and IMR reported centroid displacement in the x-axis (upper), y-axis (mid) and difference plot (lower)

some that have been used clinically such as kV/MV triangulation [10] and Kilovoltage Intrafraction monitoring (KIM) [11, 17]. There is also a commercial EMR based 3D system: Calypso (Varian Medical Systems, Palo Alto, CA, USA). A comparison with 3D systems is beyond the scope of this work and will be reported on elsewhere.

Another limitation of the IMR system is the comparably low frame rate. The IMR system takes about 2.5 s for image processing and detecting the fiducial markers for position assessment. Therefore, the frequency of image acquisition (frame rate) is limited to one image per 3 s. This differentiates IMR from other system which can observe motion in (near) real time, such as Calypso. The clinical impact of noticing a relevant motion later depends on the specifics of the case and in particular on the dose rate. For high dose rates, a more significant part of the treatment may have passed before a shift in the anatomy (fiducial markers) is noted. Unfortunately, this runs a

Table 6 Absorbed dose to water from an SBRT treatment for different scenarios (No kV imaging, MV beam on during triggered imaging, MV beam off during imaging with "gantry angle" mode and MV beam off during imaging with "time" mode)

	Absorbed dose (mGy/MU)	Treatment time (seconds)	kV images acquired (Number of frames)	Imaging dose (%)
No kV imaging	4.41	50	0	0
MV beam on during imaging	4.47	50	32	1.32
Gantry angle (18°)—MV beam off during imaging	4.47	75	32	1.32
Time (3 s)—MV beam off during imaging	4.53	100	66	2.73

Here the treatment time is the time the beam is ON plus the imaging acquisition time

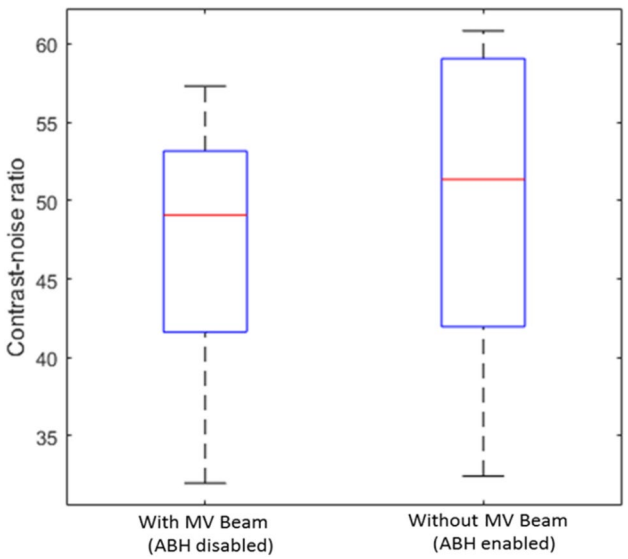

Fig. 8 Boxplot of the contrast to noise ratios (CNR) in ten kV images taken at different gantry angles with MV beam present (Auto Beam Hold (ABH) disabled) and without MV beam (ABH enabled)

contrary to the use of IMR for hypofractonated high dose rate treatments, for which it otherwise appears more suitable due to its imaging dose. However, the ability to image during treatment in near real time with a clinically available system which is integrated with Truebeam and does not require additional hardware, such as the Calypso electromagnetic array, provides clinical advantage and assurance of correct treatment location, even at a less than ideal image rate. It is certainly better than post treatment CBCT verification of the motion.

Furthermore, patient size can also effect the marker position segmentation as shown in Fig. 3. With increasing patient, size the sensitivity of IMR marker detection decreases. For clinical imaging acquisition parameters (125 kV, 15mAs), IMR detectability is 100% for patient lateral dimension up to 43 cm. The detection sensitivity can be improved by increasing the kV and mAs. However, this will result in increased patient imaging dose (see Table 7). In the clinical department in this study, patients registered for EBRT treatment for prostate cancer have, on average, have a lateral dimension of 39 cm with the largest patient lateral dimension measured at 43 cm. For patients whose largest dimension is below 43 cm, the use of 7.5 mAs in combination with 125 kV resulted in a 100% detection rate whilst minimizing the imaging dose. For larger patient dimensions, if the mAs is increased, the imaging dose can be reduced by reducing the image frequency. This is achieved by increasing the trigger interval (less image frames).

Based on marker CNR, there was no significant difference in kV image quality with or without the MV beam on (p-value = 0.51). This indicated that there is no image quality reason to pause the MV beam during triggered imaging.

A drawback of ABH with paused MV beam was an increase in overall treatment time. When using the gantry angle to trigger IMR imaging, additional time is spent as the gantry rotation pauses and backtracks after image acquisition to resume MV delivery. This adds approximately 1.5 s for each acquired frame. In the 17.5° "gantry angle" triggering

Table 7 Imaging dose per-frame for clinically significant kV-energies and mAs at the surface of the phantom and at the tissue depth of 15.3 cm

kV (imaging settings)	HVL (mmAL)	mAs (imaging settings)	$D_{w,z=0,iso}$ (mGy/frame)	$D_{w,z=15.3,iso}$ (mGy/frame)	$D_{w,z=15.3,iso}$ SBRT Boost treatment fraction (10 Gy/fraction) (mGy/fraction)
125	4.55	7.5	1.33	0.18	5.76
125	4.55	15	2.58	0.36	11.52
125	4.55	30	5.29	0.74	23.68
100	3.65	15	1.74	0.24	7.68

mode the treatment time increased from 50 to 75 s. In the "time" triggering mode, the treatment time increased even further because the "time" in IMR refers to elapsed time and not treatment (beam on) time. As the MV beam is paused before each triggered image, in the case of triggering every 3 s this resulted in twice as many images being acquired and a doubling of the treatment time from 50 to 100 s. Previous studies have shown that shortening the treatment time can reduce intrafraction motion and its effect [4] so it is important to consider treatment time and therefore the choice of trigger mode. Although potentially shortening overall treatment time, triggering by gantry angle has the disadvantage that only one image is acquired at a given gantry angle. If the markers are outside the tolerance region, no additional image is automatically acquired to assist further decision-making. However, whatever triggering mode is used, aside from the increase in imaging dose, there was no apparent effect on the delivered MV dose. In addition, as there was no significant difference in image quality when pausing the MV beam during image acquisition and therefore the reduction in the treatment delivery efficiency was not compensated by improved image quality.

The frequency of kV images is dependent on the trigger interval as shown in Table 6. With increasing trigger interval the imaging frequency decreases and hence the imaging dose decreases. Using the imaging acquisition parameters provided in Table 2 with ABH disabled, the patient would receive an additional 1.3% (11.50 mGy) dose to the prostate due to the kV imaging during a VMAT treatment as per Table 1 with 2 treatment fractions of 10 Gy. Non-target organs in the imaging field will experience a higher relative increase in dose, assuming that their dose from the MV beam is lower. The imaging dose can be reduced by altering the imaging parameters; however, this could lead to loss of fiducial marker segmentation for larger patients. Field size also has an effect on the imaging dose: Increasing the imaging field size from 6×6 cm^2 to 10×10 cm^2, the imaging dose increases by 12.3% and the volume irradiated with that dose almost triples.

Conclusion

The geometric accuracy and technical considerations for IMR use for intrafraction motion management in prostate cancer were demonstrated. IMR is a 2D real-time fiducial marker position verification system. It is able to accurately segment and report standard prostate fiducial marker positions to provide an indication of motion. Key advantages of IMR are submillimeter accuracy, full integration with the Truebeam linac with no additional external systems required and no effect on the overall MV treatment dose. Being a 2D system means that it underestimates motion in the left–right and superior-inferior directions for all kV imaging angles that are not perpendicular to the motion. Another disadvantage is that IMR delivers additional imaging dose to the patient, however, several approaches to reduce the patient-imaging dose have been provided.

Acknowledgements This work was supported and funded by a research Grant from Varian Medical System.

Funding This study was funded by the Varian Medical systems (Research and Collaboration Approval)

Compliance with ethical standards

Conflict of interest The authors declare that they have no conflict of interest.

Ethical approval This article dose not contains any studies with human participants or animals performed by any of the authors. Any patient data set was generated in routine clinical treatment and was de-identified for this purpose. Ethics approval was given by HREC for the Prometheus trial.

References

1. Olsen J, Parikh PJ, Watts M, Noel CE, Baker KW, Lakshmi S, Michalski JM (2012) Comparsion of dose decrement from intrafraction motion for prone and supine prostate radiotherapy. Radiother Oncol 104(2):199–204
2. Van Herk M, Remeijer P, Rasch C, Lebesque J (2000) The probability of correct target dosage: dose-population histograms for deriving treatment margins in radiotherapy. Int J Radiat Oncol Biol Phys 47(4):1121–1135
3. Poulsen PR, Cho B, Sawant A, Keall PJ (2010) Implementation of a new method for dynamic multileaf collimator tracking of prostate motion in arc radiotherapy using a single KV imager. Int J Radiat Oncol Biol Phys 76(3):914–923
4. Li JS, Lin M-H, Buyyounouski MK, Horwitz EM, Ma CM (2013) Reduction of prostate intrafractional motion from shortening the treatment time. Phys Med Biol 58(14):4921–4932
5. Baler M, Behrens CF (2016) Determining intrafractional prostate motion using four dimensional ultrasound system. BioMed Central Cancer 16:484
6. Schlosser J, Salisbury K, Hristov D (2012) Online image-based monitoring of soft-tissue displacements for radiation therapy of the prostate. Int J Radiation Oncol Biol Phys 83(5):1633–1640
7. Ghilezan MJ, Jaffray DA, Siewerdsen JH, Van Herk M, Shetty A, Sharpe MB, Jafri SZ, Vicini FA, Matter RC, Brabbins DS, Martinez AA (2005) Prostate gland motion assessed with cine-magnetic resonance imaging (cine-MRI). Int J Radiat Oncol Biol Phys 62(2):406–417
8. Balter JM, Wright JN, Newell LJ, Friemel B, Dimmer S, Cheng Y, Wong J, Vertatschitsch E, Mate TP (2005) Accuracy of a wireless localization system for radiotherapy. Int J Radiat Oncol Biol Phys 61(3):933–937
9. Cho B, Poulsen PR, Sloutsky A, Sawant A, Keal PJ (2009) First demonstration of combined kV/MV image-guided real time DMLC target tracking. Int J Radiat Oncol Biol Phys 74(3):859–867
10. Hunt MA, Sonnick M, Pham H, Regmi R, Xiong J-P, Morf D, Mageras GS, Zelefsky M, Zhang P (2016) Simultaneous MV-kV

imaging for intrafractional motion management during volumetric-modulated arc therapy delivery. J Appl Clin Med Phys 17(2):473–486
11. Ng JA, Booth JT, Poulsen PR, Fledelius W, Worm ES, Eade T, Hegi F, Kneebone A, Kuncic Z, Keall PJ (2012) Kilovoltage intrafraction monitoring for prostate intensity modulated arc therapy: first clinical results. Int J Radiat Oncol Biol Phys 84(5):e655–e661. https://doi.org/10.1016/j.ijrobp.2012.07.2367
12. Huang E, Dong L, Chandra A, Kuban DA, Rosen II, Evans A, Pollack A (2002) Intrafraction prostate motion during IMRT for prostate cancer. Int J Radiat Oncol Biol Phys 53(2):261–268. https://doi.org/10.1016/S0360-3016(02)02738-4
13. Timischl F (2014) The contrast-to-noise ratio for image quailty evaluation in scanning electron microscopy. J Scan Microsc 37:54–62
14. Crocker JK, Ng JA, Keall PJ, Booth JT (2012) Measurement of patient imaging dose for real-time kilovoltage x-ray intrafraction tumour position monitoring in prostate patients. Phys Med Biol 57(10):2969–2980
15. Legge K, Greer PB, Keall PJ, Booth JT, Arumugam S, Moodie T, Nguyen DT, Martin J, O'Connor DJ, Lehmannn J (2017) Technical note: TROG 15.01 SPARK trial multi-institutional imaging dose measurement. J Appl Clin Med Phy 18(5):358–363
16. Klevenhagen S, Aukett R, Harrison R, Moretti C, Nahum A, Rosser K (1996) The IPEMB code of practice for the determination of absorbed dose for x-rays below 300 kV generating potential (0.035 mm Al - 4 mm Cu HVL; 10 - 300 kV generating potential). Phys Med Biol 41(12):2605–2625
17. Keall PJ, Nguyen DT, O'Brien R, Caillet V, Hewson E, Poulsen PR, Bromley R, Bell L, Eade T, Kneebone A, Martin J, Booth JT (2018) The first clinical implementation of real-time image-guided adaptive radiotherapy using a standard linear accelerator. Radiother Oncol 127(1):6–11

Publisher's Note Springer Nature remains neutral with regard to jurisdictional claims in published maps and institutional affiliations.